Natural Hazards (2021) 105:3039–3057
https://doi.org/10.1007/s11069-020-04440-8

ORIGINAL PAPER

Co-seismic deformation and slip distribution of 5 April 2017 Mashhad, Iran earthquake using InSAR sentinel-1A image: implication to source characterization and future seismogenesis

Sanjay K. Prajapati[1] · **O. P. Mishra**[1]

Received: 13 April 2020 / Accepted: 19 November 2020 / Published online: 11 January 2021

Abstract
We analyzed interferometric synthetic aperture radar sentinel-1A-based observations to characterize the source of 5 April 2017 Mashhad, Iran mainshock (Mw 6.1), for the first time to understand the seismogenic potential of the source area using the estimates of co-seismic displacement and slip distribution on applying the steepest descent method (SDM). SAR pixel offsets (SPO) provided a deep insight into the co-seismic surface deformation of the entire source zone. Based on iterations of a total of 451 models, our analysis of sentinel-1A data from ascending and descending tracks revealed surface deformation occurred in an area of 40×30 km with a maximum co-seismic uplift of 10 cm. We estimated geodetic moment of 1.9×10^{20} Nm corresponding to the magnitude (Mw 6.0) of the Mashhad mainshock for which the rupture has a planner geometry with uniform slip dislocation in an elastic half-space with slip of 0.35 ± 0.1 m; strike of N313°E having dip of 48° of the thrust fault associated with oblique motion. The rupture length of 45 ± 3 km along-strike and 30 ± 3 km down dip has been estimated. The best-fit fault model geometry derived from SDM suggests that rupture occurred in the vicinity of the Kashafrud thrust fault, located west to the main Kopeh-Dagh Fault with its strike of 315°E. It is observed that a maximum slip of 0.35 m occurred at a depth of 8 km that extended to 10 km in the crust, which is found to be in unison to the Coulomb stress model that showed low-stressed zone is associated with the majority of events of lower magnitude ($M \leq 4.5$) in NE–SW to the mainshock, whilst the EW zone to the mainshock found relatively highly stressed as a probable source for generating relatively higher magnitude earthquakes ($M > 4.5$) in the future. We infer that the estimates of co-seismic source attributes are essentially important for understanding the nature and extent of earthquake risks for Mashhad, Iran earthquake source area and of the areas of analogous geotectonic settings, elsewhere in the world.

Keywords InSAR · Co-seismic surface deformation · Geodetic moment · Coulomb stress · Seismogenic potential · Earthquake risks

✉ O. P. Mishra
omp.mishra@nic.in

[1] National Centre for Seismology, Ministry of Earth Sciences, New Delhi, India

1 Introduction

The 5 April 2017 earthquake (MW 6.1) occurred on thrust fault located at 50 km SE to the Mashhad city of northeast Iran. This event occurred on the NW–SE active thrust fault zone named Kashafrud fault, extending between the Kopeh-Dagh and Allah Dagh-Binalud mountain ranges (USGS 2017) as shown in Fig. 1. The study region is seismically most active (Nemati et al. 2013) region of northeast Iran, which has undergone crustal shortening due to convergence between Arabian and Eurasian plates (Fig. 1). Their convergence is principally taken up by the active Makran subduction zone to the South. The estimated GPS-derived rate of the of Arabia plate with respect to Eurasia is 22 ± 2 mm/yr (Sella et al. 2002; McClusky et al. 2003; Vernant et al. 2004; Reisinger et al. 2006). At the southern boundary of the Iranian plateau, the active Makran subduction zone is accommodating a significant portion of the convergence at a rate of 13–19 mm/yr (Vernant et al. 2004). Based on the seismicity and regional geological studies, the study region is associated with predominantly with active thrust faults (Kopeh-Dagh and Allah Dagh- Binalud mountains) parallel to the strike of the isolated deforming zone without significant strike-slip faulting (Berberian and Yeats 1999; Hollingsworth et al. 2008; Jackson and McKenzie 1984). Most recent studies also documented that the source region is associated with transpressional stress regime (Mousavi et al. 2019; Aflaki et al. 2019). In recent times, there is no evidence of occurrence of earthquakes of magnitude $\geq$ Mw 6.0; however, July 1673 witnessed most destructive earthquake that occurred in Mashhad region of Iran, which destroyed two-third of Mashhad city (Ambraseys and Melville 1982). Paleo-seismological study revealed that a total of four earthquakes (M 7.0) occurred between 1209 and 1405, which were located significantly away from the present source zone and confined to the west of the Mashhad region of the Iran (Berberian and Yeats 1999).

It is worth mentioning that the study region is the second most populated region in Iran, besides it has high seismic potential associated with deformational history of the region in the Iran that has experienced at least nine large earthquakes ($M \geq 7$) during the last six centuries (Tchalenko 1975; Ambraseys and Melville 1982; Berberian and Yeats 1999, 2001) that augment the fact that any region associated with such factors makes it seismically vulnerable to promote high degree of earthquake risks in the region (Mishra 2012; Mishra et al. 2020).

The recent earthquake was accompanied by ground cracking and was followed by a complex aftershock sequence. In this paper, we utilized interferometric synthetic aperture radar (InSAR) Sentinel-1A data to examine possible dislocation model for the event that dictated the ground rupture and the aftershock sequence, which helped recognize a preferred source mechanism. Our study shed enough light on the constraint of estimating the source parameters of the mainshock in sense that the nature and extent of future seismogenesis and earthquake risk potential can be estimated through the apt characterization of the Mashhad earthquake source region and of the region of analogous seismotectonic settings, elsewhere in the world.

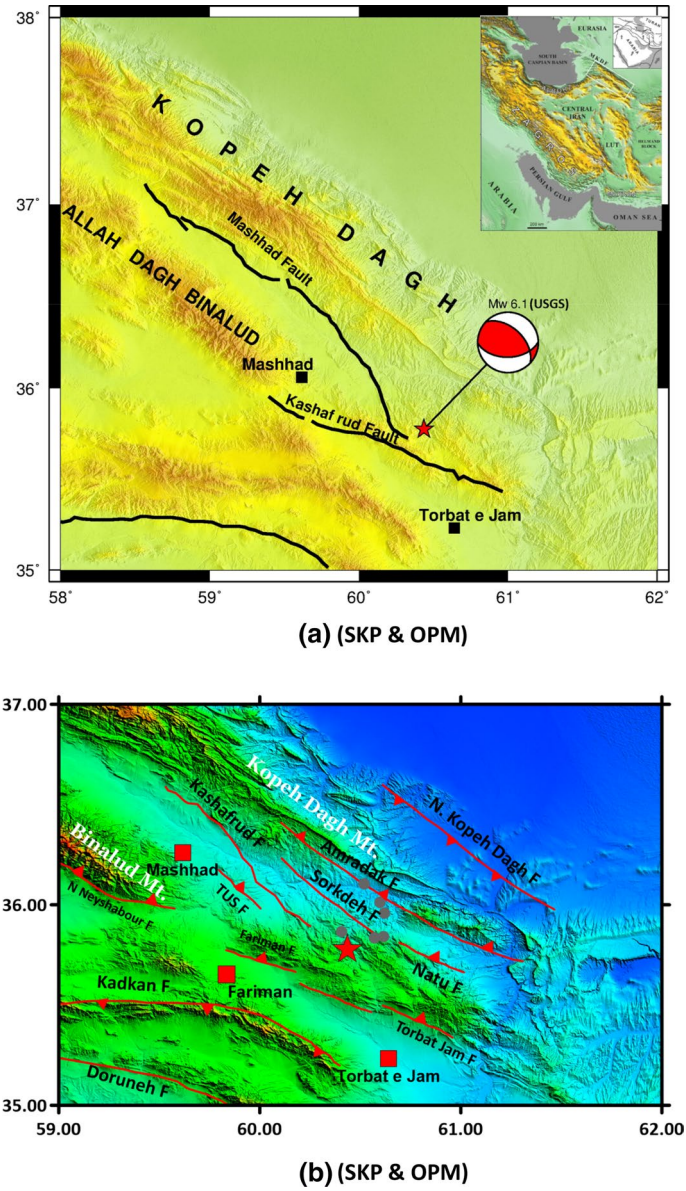

Fig. 1 **a** Shaded relief map of eastern Iran showing major faults. Black squares show major cities of eastern Iran. Red star shows the Mashhad earthquake occurred on 5th April 2017. Black solid line shows the major and active fault of NE and central Iran; **b** the distinct tectonic settings of the inset map as shown under (**a**)

2 InSAR data and analysis

To examine the ground displacements associated with this earthquake sequence, we prepared interferograms using SAR data acquired by the Sentinel-1A (C-band radar, wavelength 5.6 cm). We assimilated ascending interferograms using the 24 March 2017

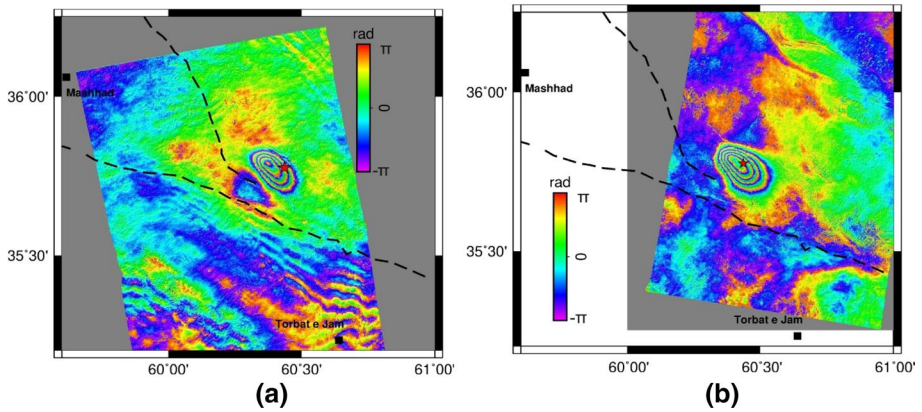

Fig. 2 **a** Co-seismic unwrapped ascending interferogram from the Mashhad earthquake (Mw 6.1, 5 April 2017) **b** Co-seismic unwrapped descending interferogram from the Mashhad earthquake (Mw 6.1, 5 April 2017). Red star shows the epicenter of Mashhad earthquake. The earthquake appears as a NW–SE elongate elliptical feature at the center of the images

and 04 April 2017 images. Descending interferograms were also prepared using 25 March 2017 and 06 April 2017 images using the approach of Sandwell et al. (2011a, b) [radar looking east, Fig. 2a; radar looking west, Fig. 2b]. Perpendicular baseline separation between the satellite orbits was found to be 35 m for the descending and 62 m for the ascending interferograms. We removed the topographic phase using a SRTM digital elevation model so that the phase in the interferograms represents ground displacements in radar line-of-sight (LOS) direction. Interferograms were unwrapped and then plotted rewrapped with each fringe representing 5.6 cm of line-of-sight (LOS) displacement. Decrease in LOS corresponds to motion toward the satellite, whilst increase in LOS indicates motion away from the satellite (Fig. 3a–b). We observed that there exist distinct differences in co-seismic fringes appearing in ascending and descending

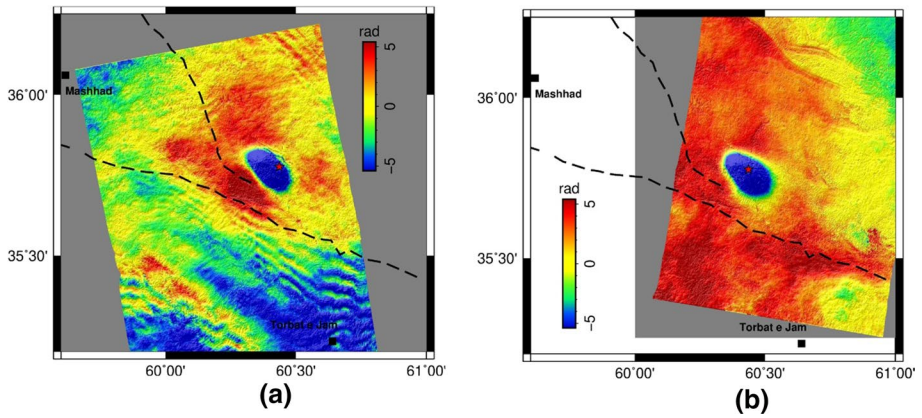

Fig. 3 Line-of-sight (LOS) displacements shown use the convention that positive motion is toward the satellite. **a** Detail of unwrapped ascending line-of-sight interferograms **b** Unwrapped descending line-of-sight interferograms

interferograms because of differences in the imaging geometry between the two acquisitions. For the ascending interferograms (Fig. 3a), the heading (azimuth) of the satellite orbit is ~100° and the look angle is approximately constant at 55°. However, for the descending interferograms (Fig. 3b), the heading angle is ~100° and the look angle changes over the swath, ranging from about 44° when both imaging geometries have approximately similar sensitivity to vertical displacements. The east–west motions have a different influence on the ascending and descending tracks, resulting in different fringe patterns. One cycle of phase difference corresponds to 2.8-cm LOS displacement. The unit vector in LOS direction for east, north, and "up" (Vertical) coordinate system is found to be 0.29, 0.07, and 0.95, respectively, whilst the corresponding values for east, north, and "up" (vertical) coordinate system are found to be 0.34, 0.08, and 0.94, respectively, for the descending interferograms. This shows that the Sentinel Radar-1A is most sensitive to vertical displacement and least sensitive to north–south displacement. East–west-oriented displacement is the principal cause of LOS displacement with an opposite sign for descending and ascending interferograms.

It is further noted that the interferometric phase in the descending and ascending interferograms (Figs. 3a–b) looks very clear and undisturbed, which suggests that dry environmental conditions in study area are very much favorable for InSAR measurements (Amelung et al. 1999). Our analysis revealed that the main phase in both the descending and ascending interferograms covers elliptical-shaped area with the increase in three color fringes that located between the north-northwest-trending active fault and aftershock zone of the mainshock. This feature characterized by an elliptical-shaped phase pattern in NW–SE with high gradient change to southeast (Fig. 3a). The similar elliptical-shaped phase pattern has also been observed for both interferograms, indicating that the ground displacement has vertical subsidence. The descending interferogram shows 2.5 cm in range that suggests uplift of 0.8 fringe, characterized by yellow-red-blue-green color, whilst the ascending interferogram shows an increase of 2.8 cm in range to the west of the teardrop with uplift of 1 fringe, characterized by red-blue-green color. These observations provided a clear insight into the degree of deformation at the surface due to co-seismic displacement.

3 Co-seismic slip modeling

We estimated fault-slip distribution of the 5 April 2017 Mashhad mainshock (Mw 6.1) from the co-seismic displacement using InSAR- Sentinel-1A observational data. In order to visualize the ascending and descending Sentinel-1A (S1A), synthetic aperture radar (SAR) data have been utilized as the principal data source for mapping the co-seismic surface deformation. We presume that the InSAR data account for the deformation only due to slip on the active thrust fault. We choose a rectangular fault plane that follows the trace of fault of 60 km, extending in down dip of 30 km. The dip angle of the plane found varied from 40° to 60°.

In order to estimate the source depth, we calculated the Green function using the dislocation theory (Okada 1992) in the multilayered earth model (CRUST 2.0) of Mooney et al. (1998) with varying impedances. We adopted the inversion scheme of Wang et al. (2009) that involved the steepest descend approach (SDM) for constrained least-square optimization, which is an iterative algorithm used for making estimate of source parameters in this study. The physical constraint is introduced to get a smooth slip model, which is realized through a roughness term that gets minimized with respect to misfit of data. The

smoothening is applied to stress drop on the whole fault by assuming a fairly smooth stress drop within slip asperities. The strike (315°) and dip (50°) of the rupture plane are assumed to be consistent with the fault plane solution of the mainshock. We considered slip distribution on a 60×30 km^2 rupture, which has sub-faults of size 2×2 km^2. The slip on each of the sub-faults is assumed to be uniform. We allowed the rake of slip on each sub-fault with variability of $\pm 10°$. As discussed above, one of the requirements in the inversion scheme is to estimate the smoothening parameter. We chose the smoothening factor based on the trade-off curve between the stress roughness of the model and the fitting residual (Fig. 4). Based on this, we found our appropriate smoothening factor is of 0.02 at the point of very sharp changes in the pattern where the curvature takes its maximum form (Fig. 4) that helped obtain our final slip model. We found that the higher value of smoothening factor, more than 0.02, provides higher misfit, but smoother slip distribution. In contrary to that the lower value of smoothing factor did not improve the misfit, while the slip distribution becomes more discrete, in order to validate our estimated co-seismic deformations from the ascending and descending interferograms are compared with those simulated using the initial fault parameters as shown in Fig. 5. Figure 5a–b shows the observed, modeled, and residual deformations from the ascending and descending interferograms, respectively. The RMSE values between the observed and the calculated modeled deformations are found to be 4.0 and 5.2 mm for the ascending and descending acquisitions, respectively (Fig. 6). Since RMSE indicates that discrepancy exists between the observed and the calculated modeled deformations, we adopted iterative processes for achieving the plausible convergence between the observed and the calculated deformation models that yielded the best

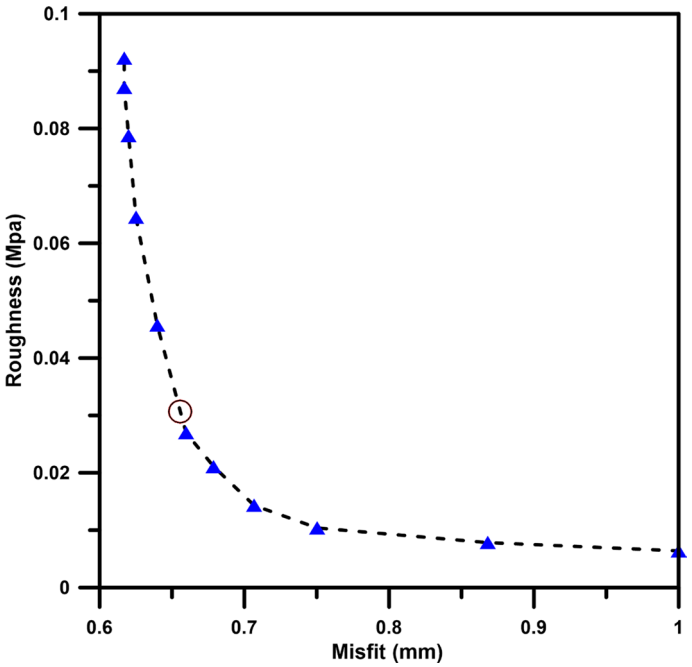

Fig. 4 Variation of roughness with average misfit between the observed and calculated values of co-seismic offsets. The inflection point in the graph corresponds to the optimum value of the smoothing parameter. In this case, we adopted a smoothing parameter value of 0.03 as marked by a circle

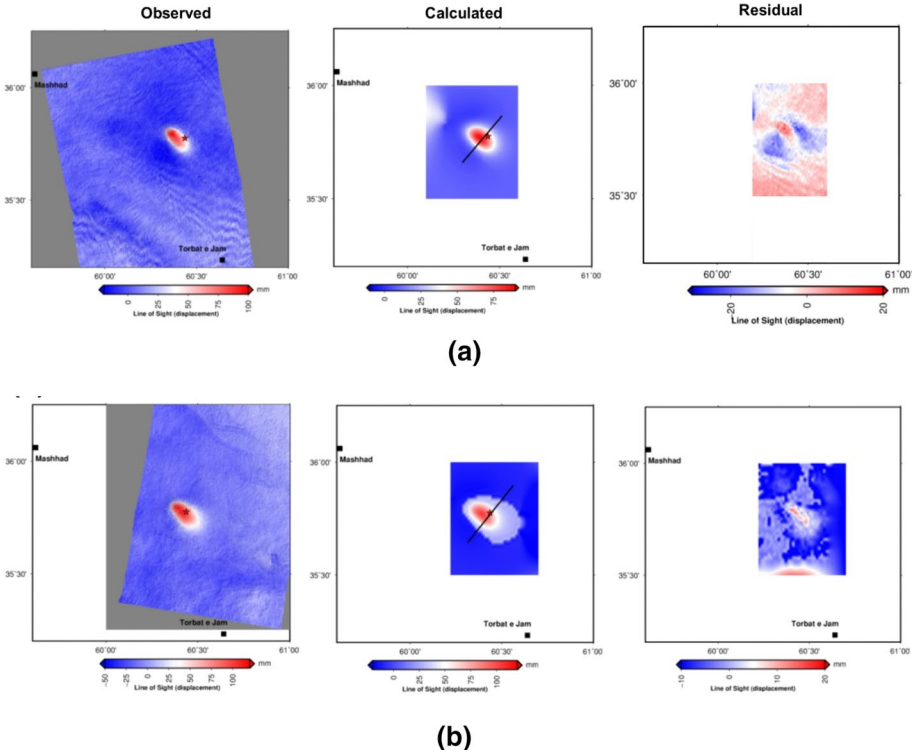

Fig. 5 Best-fitting uniform slip model of the Mashhad earthquake. (**a**) Observed, modeled and residual using ascending interferograms. (**b**) Observed, Modeled and residual using descending interferograms. Black lines show the location of the profile along which a 2D section has been drawn as shown in Fig. 6

possible and acceptable matching between the two observed and the calculated models of deformations. It is, therefore, the obtained RMSE values of 3.7 mm for the ascending interferogram and 4.6 mm for the descending interferogram (Fig. 6), which correspond to 14% of error in our estimates that may be treated as a tolerable error for estimating the co-seismic deformation of the 5 April 2017 Mashhad, Iran Earthquake (Mw 6.0). It is worth mentioning that the error estimates made by different researchers for different earthquake source zones, elsewhere in the world, showed relatively higher estimates of RMSEs that varied from 7 to 40 mm (Wang et al 2007; Motagh et al. 2010; Feng et al. 2014; Remy et al. 2015). We attempted to run a total of 451 models with different parameters that found converged for the least misfit error of 14%, which supported the matching of the observed data with our assimilated final model for estimated depth of 8 km of the mainshock. It is so because the depth of the earthquake source plays an important role in obtaining the true model. It is, therefore, we made several trials with varying models with varying depths from 5 to 35 km. The best-fit model suggests that a maximum slip occurred at a depth of 8 km of the mainshock (Fig. 6).

The extent of the residual deformation (− 10–20 mm) was much smaller than that of the modeled deformation (− 10–100 mm) for the ascending and descending interferograms (Fig. 5a–b) that reproduced uplift area very well. In particular, as seen in Fig. 5a–b, the extent of the modeled deformation was very similar to that of the observed deformation.

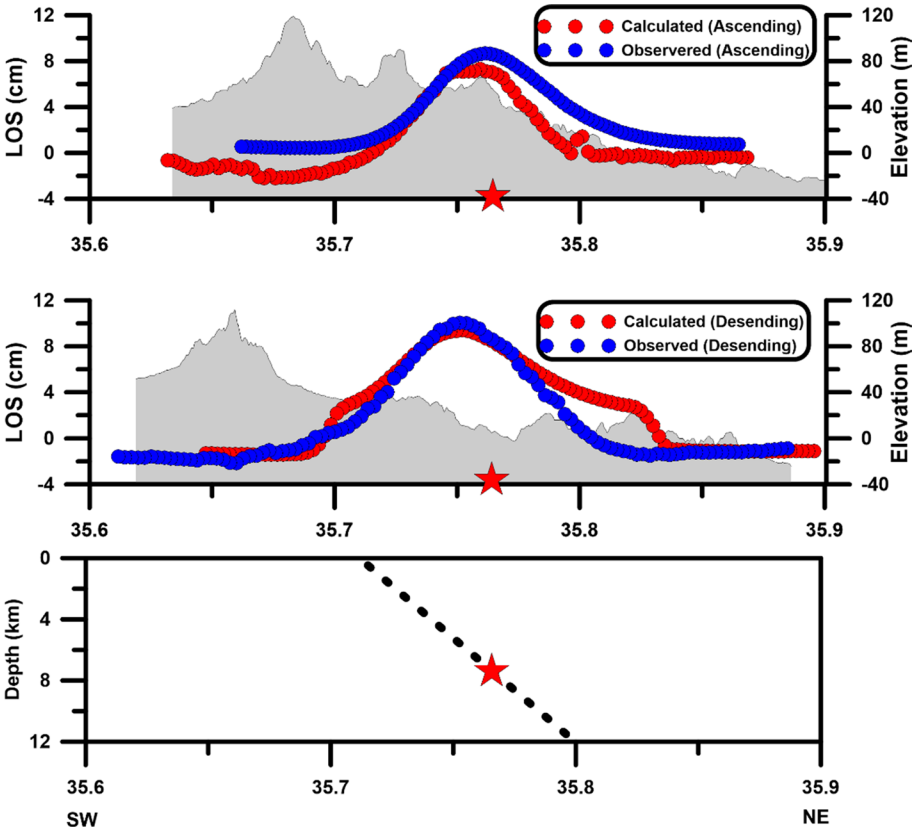

Fig. 6 Plot of observed and modeled LOS profiles parallel to the fault strike as marked in Fig. 5a, b. The blue and red lines indicate the observed and modeled line-of-sight displacement. The topography along the profiles is also shown as a light gray color in background. The location of the 5 April 2017 Mashhad Mainshock with InSAR based estimate of Magnitude (Mw 6.0) is shown by red star in all of three plots. The bottommost plot is showing the location of the mainshock in a dipping fault plane at the depth of 8 km where the slip is estimated to be maximum as shown in Fig. 7

The best-fit model for the earthquake is found to be happened for the InSAR based estimate of magnitude (Mw 6.0), and the rupture produced maximum slip of about 0.35 m that found concentrated at a depth of 8 km with the distance of about 6 km west to the epicenter (Fig. 6). It may be noted that depth estimate of the mainshock made earlier using seismological data by other agencies was significantly different (~ 12 km) for Mw 6.1 (Table 1) by USGS. It is observed that the slip on rupture extended toward southwest in the up-dip direction with respect to the strike of the Kashafrud fault (Fig. 7).

4 Static coulomb stress (ΔCFF)

Coulomb failure stress (CFS) changes from mainshocks along the causative fault planes occur because of the co-seismic deformation and that can play a significant role in triggering slip in neighboring seismic zones (King et al. 1999; Stein et al. 2010; Su et al.

Table 1 Source parameters of the 5 April 2017 Mashhad, Iran Earthquake (Mw 6.0) estimated using different data

Event	Strike (in degree)	Dip (in degree)	Rake (in degree)	Depth (km)	Moment magnitude (N-m)	Mw	Estimator agency
5 April 2017 Mashhad earthquake	315	52	120	8.0	2.57e + 18	6.0	Present study using InSAR data
	316	20	120	11.6	2.84e + 18	6.1	USGS earthquake catalogue
	101	56	58	6.0	9.813E + 17	5.9	Iranian Seismological Centre (Institute of Geophysics)

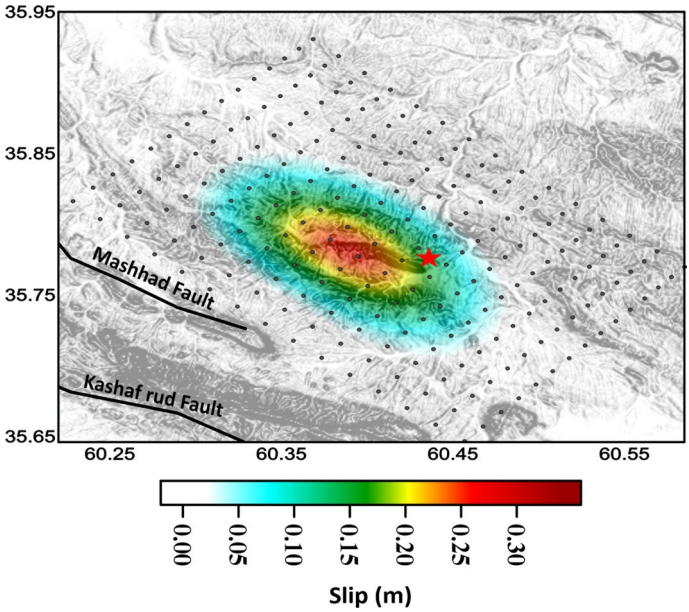

Fig. 7 Slip distribution model for the 5 April 2017 Mashhad earthquake obtained from simultaneous inversion of ascending and descending InSAR data. The distribution of tectonic features and faults is also shown in the map

2018), which may be the cause of occurrence of aftershocks. Our co-seismic slip model has been obtained using InSAR sentinel-1A imaging that shows significant displacement occurred on a shallow, elongated, northwest-trending Kashafrud fault. Early aftershocks mostly occurred in the direction perpendicular to the causative fault and concentrated in the narrow zone. In order to confirm the causative fault as the source of the mainshock and its aftershocks activity in perspective to future seismogenesis, we examined the Coulomb stress change associated with the mainshock. A series of studies during the past years showed that the static stress interactions among earthquakes control the occurrence and timing of future events (King et al. 1994; Stein 1999; King and Bowman 2003). Earthquakes tend to occur on faults where failure has been encouraged by previous events (stress triggering) and tend to avoid faults where failure has been discouraged by this trend (Amelung and Bell 2003; Mishra et al. 2013). Whether failure of a fault has been encouraged or discouraged that can conveniently be measured in terms of the Coulomb failure stress change. $\Delta\sigma_f = \Delta\tau + \mu\Delta\sigma_n$, with $\Delta\tau$ the shear stress change on the fault (positive in the slip direction), $\Delta\sigma_n$ the normal stress change on the fault (positive if the fault is normal stress) through unclamping that encourages the failure to occur, μ is the effective fault friction coefficient on the receiver fault.

The Coulomb failure stress change occurs due to the occurrence of the mainshock and its aftershocks in the source zone as shown in Fig. 8. We used the mainshock dislocation parameters derived by the finite slip model. It can be seen from Fig. 8 that most of the north-northeast-trending aftershocks occurred in an area where the Coulomb failure stress was found varying from 0.04 to − 0.1 bar, suggesting that those aftershocks (Table 2) might have triggered by the mainshock, which is confirmable to our model

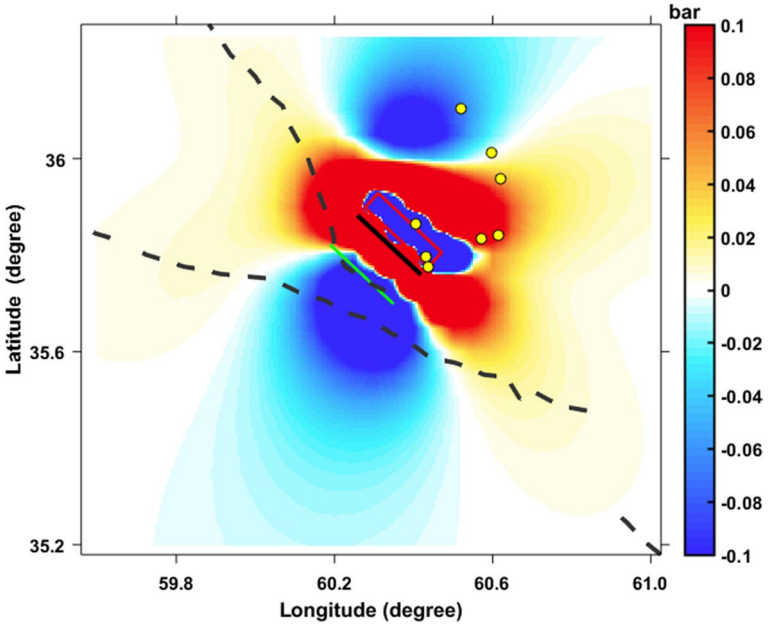

Fig. 8 Static Coulomb stress changes (in bars) due to the mainshock of magnitude Mw 6.1 calculated at a depth of 10 km with $\mu = 0.6$ and $B = 0.2$ onto a prescribed receiver fault obtained from the uniform slip model. The grid size has been taken as 0.5×0.5 km for Coulomb stress calculation. The best located aftershocks obtained from USGS (yellow circles) are also shown in this figure, the majority of them being concentrated in stress enhanced area

Table 2 List of significant aftershocks of the 2017 Mashhad, Iran Mainshock (Mw 6.1) (USGS)*

Year	Month	Day	Hour	Minute	Second	Longitude	Latitude	Depth	Magnitude
The 2017 Mashhad, Iran Mainshock (Mw 6.1)									
2017	4	5	06	09	12.2	35.7755	60.4363	13	6.1*
Some of its significant aftershocks occurred within 12 h of the mainshock and a delayed aftershock on 2017.05.02									
2017	4	5	06	19	34.74	36.0114	60.5984	10	4.8
2017	4	5	06	38	8.66	35.9573	60.6206	10	4.1
2017	4	5	07	47	30.04	35.8653	60.4061	10	4.8
2017	4	5	17	8	16.01	36.1034	60.5189	10	4.4
2017	4	5	20	7	25.82	35.7971	60.4318	10	5.1
2017	4	7	13	11	35.33	35.8421	60.6151	10	4.2
2017	5	2	21	12	11.09	35.8339	60.5704	10	5.1

*Source of the 5 April 2017 Mashhad, Iran earthquake (Mw 6.1)

derived from InSAR data. Our estimate of maximum slip at the depth of 8 km is also found concentrated in the high-Coulomb stress zone.

5 Results and discussion

We determined the geodetic moment magnitude of the 5 April 2017 Mashhad, Iran mainshock using our estimated slip distribution, which found to be Mw 6.0. The source of 5 April 2017 Mashhad, Iran earthquake (Mw 6.0) was associated with thrust fault with oblique motion on the northwest trend Kashafrud fault. Using SAR offsets, we have extracted a synoptic view of the surface displacements covering the whole epicenter area of the 5 April 2017 Mashhad earthquake source zone. Interferometric analysis of Sentinel-1A data from an ascending and a descending track reveal co-seismic ground deformation due to the Mashhad earthquake (Mw 6.0) that corresponds to seismic moment of 2.57×10^{18} Nm (Table 1) over an elliptical region of 40×30 km with a maximum co-seismic uplift of ~ 10 cm. The availability of interferograms in both ascending and descending tracks provided a good constraint for modeling the rupture zone of the mainshock that captured the deformation from two different directions. From simple elastic modeling in which we assumed that the rupture occurred in a planar uniform slip dislocation in an elastic half space. An inversion strategy has been employed to determine its source parameters (magnitude; depth of maximum slip) and variable slip distribution which comprises a nonlinear inversion for determining the fault geometry and estimating the slip distribution along the ruptured fault plane. Figure 5a–b shows observed and simulated interferograms from the optimal slip distribution and the calculated residuals. The best-fit slip distribution agrees well with observed displacements with small root mean square (RMS) misfits: 4.0 mm to LOS range changes. The model suggests the maximum slip of 0.35 m; strike of N315°E; dip of 52°; rake of 120 at source depth of 8 km (Table 1) with dimensions of 40 ± 3 km along-strike and 30 ± 3 km in down dip (Fig. 7) and shed reproduce the main features of the observed displacement. The location of our preferred rupture plane suggests that the mainshock occurred at its northeast corner and propagated southwestward. The slip model is supported by the Coulomb stress model, which suggests that the southwestward movement of the mainshock rupture has correspondence to the event occurred on a NE-dipping thrust fault. We also examined the depth of maximum slip along the NW–SE fault plane. The model shows the maximum slip that occurred at a depth of 8.0 km. Our estimate parameters of source parameters are found to be compatible with those estimated by Su et al. (2018) and Aflaki et al. (2019) except their smaller estimates of maximum slip associated with shallow depth layers having variation between 2.5 and 5.5 km, besides our fault parameters have higher dip angle of 52° that supports our model of dominantly reverse kinematics.

Based on rigorous analysis, we assimilated a schematic model of stress changes due to the occurrence of the mainshock (Mw 6.0) at a depth of 10 km with $\mu=0.06$ as $\beta=0.2$ on a fault responsible for generating the event with uniform slip. We calculated Coulombs stress (Fig. 8), which demonstrates the interrelationship between distribution of earthquakes ($2.0\leq M\leq5.0$) and the structural heterogeneity of the source region and is found in unison with the other earthquake source zones (Mishra 2012; Lei et al. 2012; Zhao 2015). The analysis of static Coulomb stress and its computation for slip provide the present stress distribution in and around the source zone, which can easily be demonstrated by a schematic model of current seismogenesis (Fig. 9a). It is well documented that the post-seismic

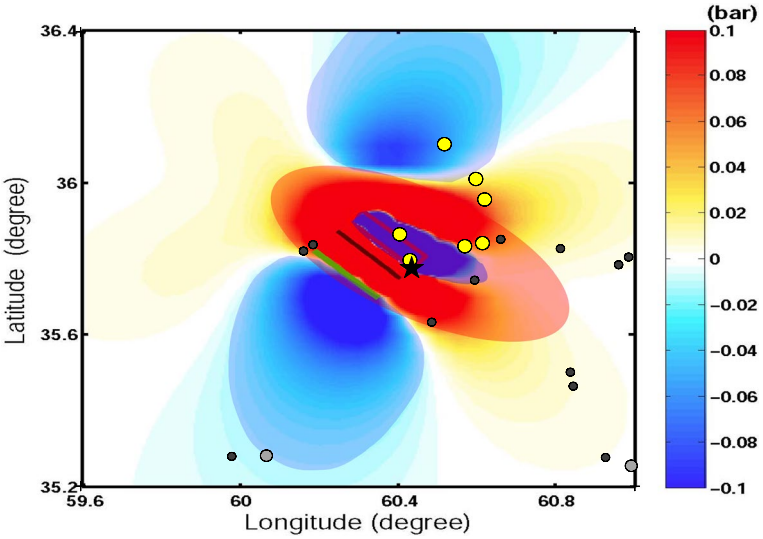

(a)

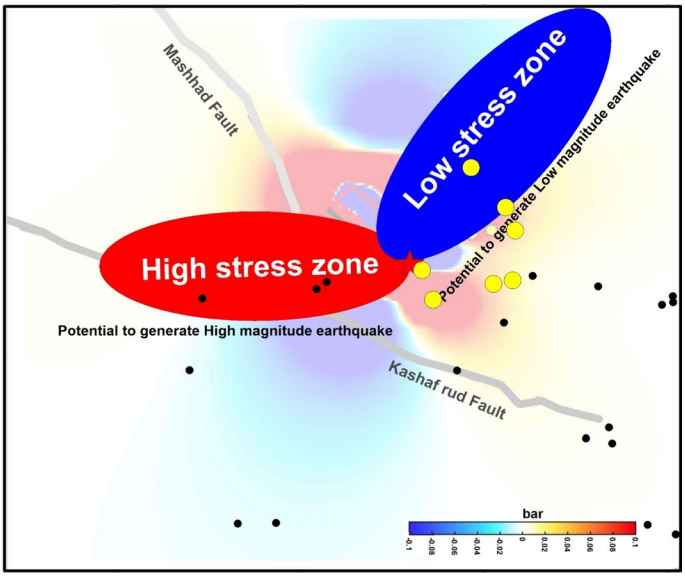

(b)

Fig. 9 (**a**) A schematic model of the source zone for seismogenesis with respect to the nature and extent of stressed regime in and around the 5 April 2017 mainshock (Mw 6.1); (**b**) A schematic model that depicts the future source zone for seismogenesis having potential to generate earthquakes of higher magnitude. The yellow circles indicate the aftershocks of the Mashhad mainshock, while the dark circles are past background earthquakes reported for the region

deformation and stress buildup have significant implications on the earthquake cycle and may increase the recurrence interval of large earthquake.

It is pertinent to note that InSAR-based estimate of magnitude of the mainshock is found to be Mw 6.0, which is slightly lower than that of the magnitude (Mw 6.1) based on estimate using seismological data from various agencies (Table 1). It is, therefore, we infer that our InSAR-based estimates of magnitude and depth of maximum slip have better constraint on our estimates of source parameters. This observation shed a light on the fact that the aftershock sequence of the 5 April 2017 mainshock might have confined to a very less number of aftershocks despite 40×30 Sq km of rupture dimension having maximum amount of slip of 0.35 m in the southwest direction to the mainshock where none of aftershocks occurred which is associated with very-high-Coulomb stress. In contrary to that aftershocks found associated with northeastward to the mainshock zone, which is found as the juxtaposition of low-Coulomb and high-Coulomb stress regime (Figs. 8, 9a). It may be because of insufficient amount of seismic energy that did not able to bring large-scale brittle failure to cause a series of aftershocks.

It is observed that a release or leakage of stress in and around the source zone may affect the future scenario of seismogenesis (Mishra 2014; Mishra et al. 2014, 2020) with respect to static Coulomb stress distribution in the source region. We further infer that high-stressed zone (Fig. 9b) is associated with a smaller number of earthquakes of relatively higher magnitude, whilst the low-stressed zone is associated with relatively more number of events of the lower magnitude. Occurrence of the mainshock in association with its aftershocks leads to the heterogeneous changes in the Coulomb failure stress from 0.04 bar to − 0.1 bar where maximum number of aftershocks (Table 2). The recent study by Su et al. (2018) demonstrated that the western and eastern walls of the seismogenic fault were sufficiently moved to the northwest where right-lateral strike-slip displacement reached to a maximum value during the Mashhad earthquake, speculating the dextral disturbance along the unknown fault may have been driven by the Mashhad mainshock and the adjacent seismogenic Tus fault could have played an important role in the strain partitioning in the region. This observation of Su et al. (2018) supports our interpretation that the seismogenic behavior of the source zone might have played a crucial role in genesis of the mainshock and its aftershocks, associating with changes in CFS as shown in Fig. 8. The maximum amount of slip of 0.35 m occurred at a depth of 8 km that is extended to 10 km beneath the source zone.

It is interesting to see that our InSAR-based slip model is found to be very much corroborative with that of Coulomb stress perturbation model that showed low-stressed zone is associated with the majority of events of lower magnitude ($M \leq 4.5$) in NE to the mainshock, whilst NW zone to the mainshock is found to be relatively more stressed. Our interpretation of the Coulomb failure stress changes is found to be in a good agreement with that of Su et al. (2018) where authors speculated that calculated CFS was very much apt to trigger the genesis of an earthquake if the Kashafrud fault and its southern continuation of the Tus fault critically get stressed due to the cascading effect that might have brought the surrounding Tus fault near to failure, consequently, fewer aftershocks occurred in the decreased CFS zones. Based on this observation, we can safely comment that the highly stressed zone to the mainshock (Figs. 9a–b) might yield earthquakes of relatively larger magnitudes in comparison with that of aftershocks of the Mashhad Mainshock occurred NE to the mainshock, since the highly stressed CFS zone has not yet witnessed the leakage of stress in the recent past. Additionally, it has also been observed from the recent study by Su et al. (2018) that the western and eastern walls of the seismogenic fault were sufficiently moved to the northwest where right-lateral strike-slip displacement reached to a maximum

value during the Mashhad earthquake, speculating the dextral disturbance along the unknown fault may have been driven by the Mashhad mainshock and the adjacent seismogenic Tus fault could have played an important role in the strain partitioning in the region. This observation of Su et al. (2018) supports our interpretation that the seismogenic behavior of the source zone may have played a crucial role in genesis of the mainshock and its aftershocks, associating with changes in CFS as shown in Figs. 8 and 9. Our study is found to be in unison to the recent study discusses the control of differential strain by the nature and extent of structural heterogeneity made by different researchers for different earthquakes occurred in different regions (Gupta et al. 1996, 2001; Mishra et al. 2013; Mishra 2013; Singh et al. 2012), which clearly supports the fact that structural heterogeneity of the source zone is responsible for generating the varying degrees of Coulomb stress beneath the source zone and corresponds to the genesis of aftershocks sequence of the mainshock (Mishra et al. 2008; Zhao et al. 2002). It is further noted that the mainshock occurred at the juxtaposition of the highly stressed and low-stressed zone associating with strong coupling or cohesiveness with source material heterogeneities (Kayal et al. 2002; Mishra et al. 2003; Singh et al. 2017), suggesting that there exists apt seismogenic strength to bring the failure. Our analysis supports the concept of variability in the seismic potential, which is the function of varying strengths of seismogenic layers and being dictated by the degree of fracture and sub-surface cracks beneath the source zone (Mishra and Zhao 2003).

The present analysis allows comparison with geological features that might have influenced the rupture initiation, propagation and termination of the mainshock (Mishra et al 2008). The surface projection of this fault appears to coincide at its southern end with the location of the mapped Kashafrud fault. Based on field surveys (Ghassabian 2017), the 2017 Mashhad earthquake was associated with blind fault that did not break the surface, which is similar to the 2001 Bhuj earthquake (Mw 7.6). Minor cracks were observed at the near foot of the fault in post-earthquake field surveys (Ghassabian 2017). Such blind fault system was associated with recent earthquakes, which has similarities with patterns of faulting for other earthquakes in northeast Iran (Talebian et al. 2004) as well as in the 2001 Bhuj earthquake in NW India (Kayal et al 2002; Mishra and Zhao 2003 ; Singh et al. 2011), which is why these areas are demarcated as the areas of high seismic risk under seismic hazard zoning map of the respective country.

The mainshock found associated with reverse faulting with dextral oblique motion in the NW-trending Kashafrud fault accompanied by co-seismic ground cracking along the Kashafrud fault, which is one of the sub-parallel faults to the Kopeh-Dagh fault system. The mainshock source zone was associated with few strong aftershocks (Mw 5) following the first day of the mainshock which concentrated only in the NNE down-dip direction of the causative fault (Fig. 8). We interpret that slip on the causative fault was seismic and aseismic slips that were generated by the mainshock. There were several studies that reported to have occurred in the source region in the past (Akbari et al. 2011), but their locations are not sufficiently well constrained to corroborate the felt earthquake reports with these moderate earthquakes used in this study. We also attempted to study the surface expression of the blind fault by projecting our estimated maximum slip depth of the source zone to the surface that found well intersected to the Kashafrud fault in the vicinity of ~ 800 m. (Fig. 1), suggesting that this is the plausible causative fault that generated the 5 April 2017 Mashhad Iran earthquake with its InSAR based estimate of its moment magnitude (Mw 6.0) at a source depth of 8 km, which can be further reinforced by the morphological study of the source region associated with seismogenic fault.

We found that the source zone of the 5 April 2017 Mashhad, Iran earthquake has heterogeneous stress distribution in which the zone between Mashhad fault and Kashafrud fault

is highly stressed, and the mainshock occurred at the zone which is juxtaposition of high and low stress perturbation. This observation, in turn, suggests that the imaging of distinct stress variation and co-seismic modeling using InSAR Sentinel-1A data helped for better source characterization and its bearing on seismogenesis and rupture propagation. Our determined maximum slip of 0.35 m at source depth of 8 km, which is in a good agreement with geometric factors of the deep-seated causative fault systems (e.g., their segmentation, spacing and overlapping relations), is in continental block boundaries as shown in Fig. 1a–b.

6 Summary

InSAR is an ideal technique to identify the blind fault system in quaternary tectonically active region. In the present study, using information from both ascending and descending tracks of Sentinel -1A data, we have identified the source zone for the ground deformation associated with Mashhad, Iran earthquake of InSAR based moment magnitude (Mw 6.0). The source was associated with thrust fault with oblique motion on the northwest-trending Kashafrud fault. The mainshock was accompanied by co-seismic ground cracking parallel to fault. We also observed that the magnitude of the co-seismic event is well constrained by the InSAR data, which is mostly consistent with the magnitude (Mw 6.0) what we estimated using InSAR data and differs from that of seismological studies (Mw 6.1). We found that the majority of moment release at optimum slip depth that occurred at a depth of 8 km, derived from the uniform slip model. Interestingly, the aftershocks occurred in the juxtaposition of low and high stress zone. The depth of the maximum slip is found to be confirmable with the appreciable Coulomb stress.

The maximum slip distribution (0.35 m) corresponds to high-stressed zone with positive stress perturbation at the source depth of 8 km, which is predominantly oriented toward southwest to the mainshock, where possibility exists for occurrence of relatively high magnitude earthquakes ($M >= 6.0$). The zone in the northeast to the mainshock is found to have a negligible slip associated with low-stress regime having negative stress perturbation, which may have potential to generate relatively lower magnitude earthquakes, whilst the highly stressed zone having positive CFS can have potential of generating earthquakes of relatively larger magnitudes. It is, therefore, the source zone of the 5 April 2017 Mashhad, Iran earthquake has heterogeneous stress distribution in which the zone between Mashhad fault and Kashafrud fault is highly stressed, and the mainshock occurred at the zone which is juxtaposition of high- and low-stress perturbation. This observation, in turn, suggests that the imaging of distinct stress variation and co-seismic modeling using InSAR Sentinel-1A data helped for better source characterization and its bearing on seismogenesis and rupture propagation. The present analysis allows us to make adopt a practice for reassessment of earthquake magnitudes using the state-of-the-art technique of estimating geodetic moment magnitude (Mw 6.0) of the earthquake using the InSAR-based assimilated slip model, which in turn help comparing with geological features that might have influenced the rupture initiation, propagation and termination of the mainshock rupture, which is essentially important for understanding the nature and extent of earthquake risks for Mashhad, Iran earthquake source area and of the areas of analogous geotectonic settings, elsewhere in the world.

Acknowledgement Authors profusely thank Secretary, Ministry of Earth Sciences (MoES) for motivating and encouraging for conduction of leading-edge research, which has relevance to societal issues. Authors

gratefully acknowledge Prof. Shailesh Nayak, Director, National Institute of Advanced Studies (NIAS), India, and Former Secretary, MoES for his encouragement to conduct studies on earthquake source characterization using satellite based data for better insight into the earthquake processes. The authors are also thankful to the Director, National Centre for Seismology (NCS), MoES, India, for support and encouragement. Entire data analyses and novel interpretation have been carried out by authors at NCS, MoES, New Delhi, India. We gratefully thank Prof. R Wang for providing Fortran code for inversion of co-seismic surface deformation data (InSAR, GPS) for fault-slip distribution. The topographic contribution to the phase is removed using a digital elevation model from the Shuttle Radar Topography Mission. Sentinel-1 data are copyright of Copernicus (2016). Most of the figures were made using the GMT software (Wessel and Smith, 1998). Differential interferograms are produced using the software package GMTSAR. Colleagues of NCS, MoES are thankfully acknowledged for stimulating discussion. We are extremely grateful to two anonymous reviewers, Editor-in-Chief and the editorial office of NHZ for their useful suggestions that improved our original research article.

Author contributions SKP was involved in data scrutiny, data processing and figures generation. OPM performed data Analysis, interpretation and writing of the manuscript

Data availability The topographic contribution to the phase is removed using a digital elevation model from the Shuttle Radar Topography Mission. Sentinel-1 data are copyright of Copernicus (2016), are used for the study, and are properly acknowledged.

References

Aflaki M, Mousavi Z, Ghods A, Shabanian E, Vajedian S, Akbarzadeh M (2019) The 2017 Mw 6 sefid sang earthquake and its implication for the geodynamics of NE Iran. Geophys J Int 218(2):1227–1245

Akbari M, Ghafoori M, Moghaddas NH, Lashkaripour GR (2011) Seismic microzonation of Mashhad city, northeast Iran. Annal Geophys 54:4. https://doi.org/10.4401/ag-4771

Ambraseys N, Melville C (1982) A history of persian earthquakes. Cambridge University Press, Cambridge

Amelung F, Bell JW (2003) Interferometric synthetic aperture radar observations of the 1994 double spring flat, Nevada, earthquake (M5.9): main shock accompanied by triggered slip on a conjugate fault. J Geophy Res 108:9–2433. https://doi.org/10.1029/2002JB001953

Amelung F, Glloway DL, Bell JW, Zebker HA, Laczniak RJ (1999) Sensing the ups and downs of Las-vegas: inSAR reveals structural control of land subsidence and aquifer-system deformation. Geology 27(6):483–486

Berberian M, Yeats R (1999) Patterns of historical earthquake rupture in the Iranian Plateau. Bull Seism Soc Am 89:120–139

Berberian M, Yeats R (2001) Contribution of archaeological data to studies of earthquake history in the Iranian Plateau. J Struct Geol 23:563–584

Feng W, Li Z, Hoey T, Zhang Y, Wang R, Samsonov S, Li Y, Xu Z (2014) Patterns and mechanisms of coseismic and postseismic slips of the 2011 MW 7.1 Van (Turkey) earthquake revealed by multi-platform synthetic aperture radar interferometry. Tectonophysics 632:188–198

Ghassabian NN (2017) A report of earthquake Mw=6.1Sefid sang Mashhad 2017-04-05, Technical Report, Geological Survey of Iran

Gupta HK, Sarma SV, Harinarayana T, Virupakshi G (1996) Fluids below the hypocentral region of Latur earthquake, India: geophysical Indicators. Geophys Res Lett 23:1569–1572

Gupta HK, Rao NP, Rastogi BK, Sarkar D (2001) The deadliest intraplate earthquake. Science 291(5511):2101–2103

Hollingsworth J, Jackson J, Walker R, Nazari H (2008) Extrusion tectonics and subduction in the eastern South Caspian region since 10 Ma. Geology 36(10):763–766. https://doi.org/10.1130/G25008A.1

Jackson J, McKenzie D (1984) Active tectonics of the Alpine-Himalayan belt between western Turkey and Pakistan. Geophys J R astr Soc 77(1):185–264

Kayal JR, Zhoa D, Mishra OP, De R, Singh OP (2002) The 2001 Bhuj earthquake: tomographic evidence for fluids at the hypocenter and its implications for rupture nucleation. Geophys Res Lett 29:5–1. https://doi.org/10.1029/2002GL015177

King GCP, Bowman DD (2003) The evolution of regional seismicity between large earthquakes. J Geophys Res 108(B2):2096. https://doi.org/10.1029/2001JB000783

King GCP, Stein RS, Lin J (1999) Static stress changes and the triggering of earthquakes. Bull Seismol Soc Am 84:935–953

Lei J, Xie F, Mishra OP, Zhang G, Lu Y, Li Y (2012) The 2011 Yingjiang, China, earthquake (M 5.8): a volcano-related fluid-driven earthquake? Bull Seismol Soc Am 102:417–425

McClusky S, Reilinger R, Mahmoud S, Ben Sari D, Tealeb A (2003) GPS constraints on Africa (Nubia) and Arabia plate motions. Geophys J Int 155(1):126–138. https://doi.org/10.1046/j.1365-246X.2003.02023.x

Mishra OP (2012) Seismological research in India (2007–2011). Proc Ind Nat Sci Acad Publ (PINSA) 76(3):361–375

Mishra OP (2013) Crustal Heterogeneity in Bulk Velocity beneath the 2001 Bhuj earthquake source zone and its implications. Bull Seismol Soc Am 103(6):3235–3247. https://doi.org/10.1785/0120110144

Mishra OP (2014) Intricacies of himalayan seismotectonics and seismogenesis: need of an integrated research. Curr Sci 106(2):176–187

Mishra OP, Zhao D (2001) Crack density, saturation rate and porosity at the. Earth Planet Sci Lett 212:393–405

Mishra OP, Zhao D (2003) Crack density, saturation rate and porosity at the 2001 Bhuj, India, earthquake hypocenter: a fluid-driven earthquake? Earth Planet Sci Lett 212:393–405

Mishra OP, Zhao D, Umino N, Hasegawa A (2003) Tomography of northeast Japan forearc and its implications for interplate seismic coupling. Geophys Res Lett 30:2003. https://doi.org/10.1029/2003GL017736

Mishra OP, Zhao D, Wang Z (2008) The genesis of the 2001 Bhuj, India, earthquake (Mw 7.6): a puzzle for Peninsular India. J. Indian Min Spec Issue 61(3–4):149–170

Mishra OP, Dutta PK, Naskar MK (2013) Relationship between earthquake fault triggering and societal behavior using ant colony optimization. Adv Phys Theor Appl 26:99–108

Mishra OP, Vandana, Kumar V (2020) A new insight into seismic attenuation characteristics of Northwest Himalaya and its surrounding region: Implications to structural heterogeneities and earthquake hazards. Earth Plant. Inters, Phys. https://doi.org/10.1016/j.pepi.2020.106500

Mishra OP, Singh AP, Kumar D, Rastogi BK (2014) An insight into crack density, saturation rate and porosity model of the 2001 Bhuj earthquake in the stable continental region of Western India. J Asian Earth Sci 83:48–59

Mooney WD, Laske G, Masters TG (1998) CRUST 5.1: a global crustal model at 5°x5°. J Geophys Res 103:727–747

Motagh M, Schurr B, Anderssohn J, Cailleau B, Walter TR, Wang R, Villotte JP (2010) Subduction earthquake deformation associated with 14 November 2007, Mw 7.8 tocopilla earthquake in chile: results from InSAR and aftershocks. Tectonophysics 490(1–2):66–68. https://doi.org/10.1016/j.tecto.2010.04.033

Nemati M, James Hollingsworth Z, Zhan MJ, Bolourchi Talebian M (2013) Microseismicity and seismotectonics of the South Caspian lowlands NE Iran. 193(3):1053–1070. https://doi.org/10.1093/gji/ggs114

Okada Y (1992) Internal deformation due to shear and tensile faults in a half-space". Bull Seismol Soc Am 82(2):1018–1040

Reilinger R et al (2006) GPS constraints on continental deformation in the Africa-Arabia- eurasia continental collision zone and implications for the dynamics of plate interactions. J Geophys Res 111:B05411. https://doi.org/10.1029/2005JB004051

Remy D, Chen Y, Froger JL, Bonvalot S, Cordoba L, Fustos J (2015) Revised interpretation of recent InSAR signals observed at Llaima volcano (Chile). Geophys Res Lett 42:3870–3879. https://doi.org/10.1002/2015GL063872

Sandwell D, Mellors R, Tong X, Wei M, Wessel P (2011a) Open radar interferometry software for mapping surface deformation. Eos Trans AGU 92(28):2. https://doi.org/10.1029/2011EO280002

Sandwell D, Mellors R, Tong X, Wei M, Wessel P (2011b) GMTSAR: An InSAR Processing System Based on Generic Mapping Tools. UC San Diego: Scripps Institution of Oceanography. Retrieved from: http://escholarship.org/uc/item/8zq2c02m.

Sella GF, Dixon TH, Mao A (2002) REVEL: a model for recent plate velocities from space geodesy. J Geophys Res 107(B4):2081. https://doi.org/10.1029/2000JB000033

Singh AP, Mishra OP, Rastogi BK (2011) 3-D Seismic structure of the Kachchh, Gujarat and its implications for the earthquake hazard mitigation. Nat Hazards 57(1):83–105. https://doi.org/10.1007/s11069-010-9707-2

Singh AP, Mishra OP, Singh RB, Kumar D (2012) A new insight into Crustal Heterogeneity beneath the 2001 Bhuj earthquake region of Northwest India and its implications for rupture initiations. J Asian Earth Sci 48:31–42. https://doi.org/10.1016/j.jseaes.2011.12.020

Sigh AP, Purnachandra Rao N, Ravi Kumar M, Hsieh M-C, Zhao L (2017) Role of the kopili fault in deformation tectonics of the indo-burmese arc inferred from the rupture process of the 3 january 2016 Mw 6.7 Imphal earthquake. Bull Seismol Soc Am 107(2):1041–1047. https://doi.org/10.1785/0120160276

Stein RS (1999) The role of stress transfer in earthquake occurrence. Nature 402:605–609
Stein RS, Barka AA, Dieterich JH (2010) Progressive failure on the north Anatolian fault since 1939 by earthquake stress triggering. Geophys J Roy Astronom Soc 128:594–604
Su Z, Yang YH, Li YS, Xu XW, Zhang J, Zhou X, Ren JJ, Wang EC, Hu JC, Zhang SM, Talebian M (2018) Coseismic displacement of the 5 April 2017 Mashhad earrhquake (Mw 61) in NE Iran through Sentinel-1A TOPS data: new implications for the strain partitioning in the southern Binalud mountains. J. Asian Earth Sci. 169:244–256
Talebian M, Fielding EJ, Funning GJ, Ghorashi M, Jackson J, Nazari H (2004) The 2003 Bam (Iran) earthquake: rupture of a blind strike-slip fault. Geophys Res Lett 31:11
Tchalenko JS (1975) Seismicity and structure of the Kopet Dagh Iran, USSR. Phil Trans R Soc Lond, Series A 278(1275):1–28
USGS (2017) Strong magnitude 6.1 earthquake of northern and Central Iran on wednesday, 5 April 2017 at 06:09 (GMT), USGSTED (usgs.govearthquake) & https://www.volcanodiscovery.com/
Vernant P et al (2004) Present-day crustal deformation and plate kinematics in the Middle East constrained by GPS measurements in Iran and northern Oman. Geophys J Int 157(1):381–398. https://doi.org/10.1111/j.1365-246X.2004.02222.x
Wang H, Xu C, Ge L (2007) Coseismic deformation and slip distribution of the 1997 Mw 7.5 Manyi, Tibet, earthquake from InSAR measurements. J Geodyn 44:200–212. https://doi.org/10.1016/j.jog.2007.03.003
Wang L, Wang R, Roth F, Enescu B, Hainzl S, Ergintav S (2009) After-slip and viscoelastic relaxation following the 1999 M7.4 Ízmit earthquake, from GPS measurements. Geophys J Int 178:1220–1237
Zhao D, Mishra OP, Sanda R (2002) Influence of fluid and magma on earthquakes: seismological evidence. Phys Earth Planet Inter 132:249–267
Zhao D (2015) Multiscale seismic tomography. Springer, Tokyo, 315